The 8th European Congress on Computational Methods in Applied Sciences and Engineering
ECCOMAS Congress 2022
5-–9 June 2022, Oslo, Norway

INFLUENCES OF THE GEOMETRICAL NONLINEARITY ON THE COMPLEX BAND STRUCTURES OF PERIODIC LATTICE FRAME STRUCTURES

MARIUS MELLMANN[1], BENJAMIN ANKAY[1], ELIAS PERRAS[1] AND CHUANZENG ZHANG[1]

[1] Chair of Structural Mechanics
University of Siegen
Campus Paul-Bonatz, 57076 Siegen, Germany
e-mail: mellmann@bau.uni-siegen.de

Key words: Elastic Wave Propagation, Complex Band Structures, Periodic Frame Structures, Spectral Element Method (SEM), Geometrical Nonlinearity, Phononic Structures

Abstract. In this study, the complex band structures of geometrically nonlinear periodic frame structures are calculated by using the Spectral Element Method (SEM). For this purpose, the spectral element matrix for a geometrically nonlinear beam element is derived. By solving the inverse eigenvalue problem for computing the complex dispersion curves $k(\omega)$ instead of the conventional eigenvalue problem for calculating the real dispersion curves $\omega(k)$, the complex wave vector can be obtained, whose imaginary parts describes the evanescent behavior of the Bloch waves. Subsequently, the geometrically nonlinear effects on the evanescent behavior of the Bloch waves are investigated by evaluating the dispersion curves and the transmission spectra.

1 INTRODUCTION

In recent years, the importance of insulating or protecting buildings, machines and people from dynamic and acoustic influences has increased rapidly. Examples are the sound protection in residential buildings, soundproofing against road and rail traffic noise or the protection against noise and vibration from construction work. Particularly strict are the requirements in the field of micro- and nanotechnology, where even vibration levels of $0.5 - 6\,\mu$m/s could be problematic. Due to these increasing requirements, the development of new materials and structures with outstanding acoustic and elastodynamic properties has become a popular research field. In particular, the phononic materials and structures, shown exemplarily in Fig. 1, are very promising. These structures are characterized by a periodic arrangement of different materials or geometries. Depending on the periodicity, as also shown in Fig. 1, a distinction is made between 1D, 2D and 3D phononic structures. The increasing research interest in the phononic materials and structures is based on the unique acoustic and elastodynamic properties, namely, these structures have certain frequency ranges, referred to as the band-gaps or stop-bands, in which the elastic and acoustic waves cannot propagate. Accordingly, these materials and structures are suitable, for example, for selective sound and vibration insulation and surpass the damping properties of conventional insulating materials clearly within the frequency range of a

band-gap [1]. Compared to the conventional materials, lattice structures have a comparatively low weight with a high load-bearing capacity and are particularly popular in lightweight construction. The increasing popularity is not least due to new manufacturing techniques, such as additive manufacturing (3D printing). Periodic lattice structures can, analogous to conventional perodic materials, exhibit band-gaps and are also referred to as phononic lattice structures in this context. For example, MATLACK et al. [2] designed a 3D phononic lattice structure with

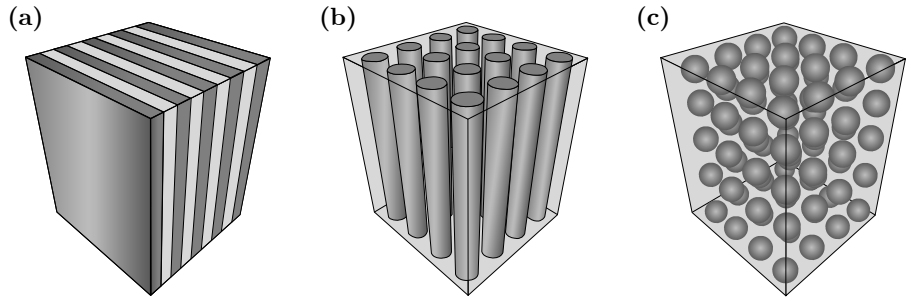

Figure 1: Examples of phononic structures: **(a)** 1D phononic structure, **(b)** 2D phononic structure and **(c)** 3D phononic structure.

broad band-gaps in the low-frequency range by combining the BRAGG scattering and the local resonance mechanisms. Due to the simultaneously low intrinsic weight such structures have promising applications, for example for vibration insulation in aerospace engineering, as illustrated in Fig. 2, or similar areas of engineering where a low weight is an important criterion. The zig-zag lattice structures, examplarily illustrated in Fig. 3 where the associated unit-cell is shown enlarged, represent a possible lattice topology in which even with homogeneous material and cross-sectional properties band-gaps can be achieved [3, 4]. The wave propagation properties of phononic zig-zag lattice structures can be tuned by many parameters, such as the amplitude of the deflection W, the lattice constants l_1 and l_2, the material properties, the cross-section properties, and others. One way of influencing the wave propagation properties

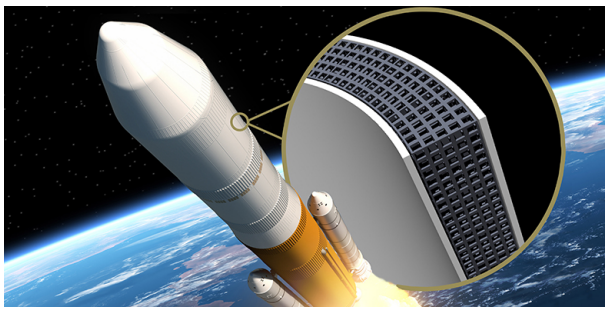

Figure 2: Phononic lattice structure for vibration insulation in a rocket. Graphic by: 3Dsculptor/Shutterstock/JUNG-CHEW TSE, ETH Zürich.

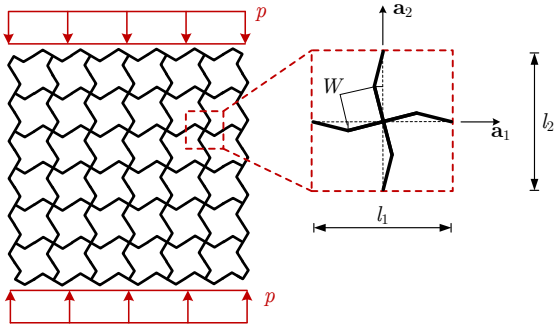

Figure 3: Example of a 2D phononic zig-zag-lattice structure under uniaxial compression p and the corresponding unit-cell.

.

adaptively is to utilize the effects of the geometric nonlinearity by applying an external load p on the lattice structure, as also illustrated in Fig. 3. In this study, the influences of the geometric nonlinearity on the complex band structures and transmission spectra of phononic zig-zag lattice structures are analyzed by using the Spectral Element Method (SEM). For this purpose, the spectral element matrix for a geometrically nonlinear beam element is derived.

2 GEOMETRICALLY NONLINEAR SPECTRAL BEAM ELEMENT

In the following, the spectral EULER-BERNOULLI beam element is derived according to the geometrically nonlinear beam theory, which, to the best of the author's knowledge, is not known in the literature in the presented form. However, some authors have already derived spectral stiffness matrices for beams that take axial forces into account. For example, BANERJEE and FISHER [5] derived the spectral stiffness matrix for a coupled bending-torsion problem considering axial forces. In addition, CAPRON and WILLIAMS [6] derived an exact dynamic stiffness matrix for the TIMOSHENKO beam on an elastic foundation considering an axial load.
The starting point for the derivation is the following equation of motion for free beam vibration

$$EI\frac{\partial^4 w}{\partial x^4} - S\frac{\partial^2 w}{\partial x^2} + \rho A\frac{\partial^2 w}{\partial t^2} = 0, \tag{1}$$

where E is the YOUNG's modulus, I is the second area moment of inertia, S is the axial force, ρ is the mass density, A is the cross-sectional area and w is the transverse displacement of the beam. Assuming a time-harmonic wave propagation, Eq. (1) can be transformed to the frequency domain, which yields

$$EI\frac{\partial^4 w}{\partial x^4} - S\frac{\partial^2 w}{\partial x^2} - \omega^2 \rho A w = 0, \tag{2}$$

where ω is the angular frequency. The following derivation of the spectral element matrix is based on the force-displacement relation method. However, the derivation can also be carried out using the state-vector equation method or the GALERKIN projection. For the derivation of the spectral shape functions, the following spectral approach for the displacement $w(x)$

$$w(x) = a\mathrm{e}^{-\mathrm{i}k(\omega)x} \tag{3}$$

is introduced. Substituting Eq. (3) into Eq. (1) leads to

$$EIk^4 + Sk^2 - \omega^2 \rho A = 0, \tag{4}$$

from which the dispersion relation

$$k^4 \pm 2\lambda^2 k^2 - k_B^4 = 0, \quad \text{with} \quad \lambda = \sqrt{\frac{|S|}{2EI}} \text{ and } k_B = \sqrt{\omega}\left(\frac{\rho A}{EI}\right)^{1/4}, \tag{5}$$

can be obtained. Here, λ is the buckling coefficient and k_B is the wavenumber for the bending or flexural wave mode according to the linear beam theory. The sign before the second term of Eq. (5) is positive if S is a tensile force and correspondingly negative if S is a compressive force.

The four zeros of the dispersion relation are given by

$$k_1 = -k_2 = \sqrt{\lambda^2 + \sqrt{k_B^4 + \lambda^4}}, \quad k_3 = -k_4 = \mathrm{i}\sqrt{-\lambda^2 + \sqrt{k_B^4 + \lambda^4}}, \tag{6}$$

if S is a compressive force, and

$$k_1 = -k_2 = \sqrt{-\lambda^2 + \sqrt{k_B^4 + \lambda^4}}, \quad k_3 = -k_4 = \mathrm{i}\sqrt{\lambda^2 + \sqrt{k_B^4 + \lambda^4}}, \tag{7}$$

if S is a tensile force. For a shorter notation, the root terms for the case of a compressive force S are substituted by

$$k_{\lambda 1} = \sqrt{\lambda^2 + \sqrt{k_B^4 + \lambda^4}} \quad \text{and} \quad k_{\lambda 2} = \sqrt{-\lambda^2 + \sqrt{k_B^4 + \lambda^4}}, \tag{8}$$

and for the case of a tensile force S by

$$k_{\lambda 1} = \sqrt{-\lambda^2 + \sqrt{k_B^4 + \lambda^4}} \quad \text{and} \quad k_{\lambda 2} = \sqrt{\lambda^2 + \sqrt{k_B^4 + \lambda^4}}. \tag{9}$$

Here, $k_{\lambda 1}$ and $k_{\lambda 2}$ can be understood as wave numbers for the bending wave modes according to the geometrically nonlinear beam theory. The general solution of Eq. (1) is therefore given by

$$w(x) = a_1 \mathrm{e}^{-\mathrm{i}k_{\lambda 1}x} + a_2 \mathrm{e}^{-k_{\lambda 2}x} + a_3 \mathrm{e}^{\mathrm{i}k_{\lambda 1}x} + a_4 \mathrm{e}^{k_{\lambda 2}x} = \mathbf{e}_{B,GNL}(x,\omega)\mathbf{a}_B, \tag{10}$$

where

$$\mathbf{e}_{B,GNL}(x,\omega) = \left[\mathrm{e}^{-\mathrm{i}k_{\lambda 1}x}\ \mathrm{e}^{-k_{\lambda 2}x}\ \mathrm{e}^{\mathrm{i}k_{\lambda 1}x}\ \mathrm{e}^{k_{\lambda 2}x}\right] \quad \text{and} \quad \mathbf{a}_B = \left[a_1\ a_2\ a_3\ a_4\right]^T. \tag{11}$$

Consequently, the nodal degrees of freedom $\mathbf{d}_{B,GNL}$ can be expressed as

$$\mathbf{d}_{B,GNL} = \begin{bmatrix} w\,(0) \\ -w'(0) \\ w\,(l) \\ -w'(l) \end{bmatrix} = \begin{bmatrix} w_1 \\ \theta_1 \\ w_2 \\ \theta_2 \end{bmatrix} = \begin{bmatrix} \mathbf{e}_{B,GNL}(0,\omega) \\ -\mathbf{e}'_{B,GNL}(0,\omega) \\ \mathbf{e}_{B,GNL}(l,\omega) \\ -\mathbf{e}'_{B,GNL}(l,\omega) \end{bmatrix} \mathbf{a}_B = \mathbf{H}_{B,GNL}(\omega)\mathbf{a}_B, \tag{12}$$

where the sign convention shown in Fig. 4 applies. The prime ($'$) denotes the derivative with

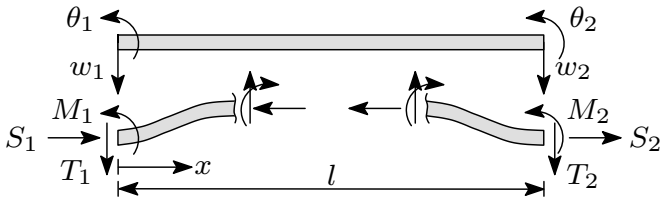

Figure 4: Sign convention of the Euler-Bernoulli beam element.

respect to x and the matrix $\mathbf{H}_{B,GNL}$ is given by

$$\mathbf{H}_{B,GNL} = \begin{bmatrix} 1 & 1 & 1 & 1 \\ \mathrm{i}k_{\lambda 1} & k_{\lambda 2} & -\mathrm{i}k_{\lambda 1} & -k_{\lambda 2} \\ \mathrm{e}^{-\mathrm{i}k_{\lambda 1}l} & \mathrm{e}^{-k_{\lambda 2}l} & \mathrm{e}^{\mathrm{i}k_{\lambda 1}l} & \mathrm{e}^{k_{\lambda 2}l} \\ \mathrm{i}k_{\lambda 1}\mathrm{e}^{-\mathrm{i}k_{\lambda 1}l} & k_{\lambda 2}\mathrm{e}^{-k_{\lambda 2}l} & -\mathrm{i}k_{\lambda 1}\mathrm{e}^{\mathrm{i}k_{\lambda 1}l} & -k_{\lambda 2}\mathrm{e}^{k_{\lambda 2}l} \end{bmatrix}. \tag{13}$$

The displacement field of the spectral beam element can now be expressed in terms of the nodal displacements and rotations $\mathbf{d}_{B,GNL}$ via the relation

$$w(x) = \mathbf{N}_{B,GNL}(x,\omega)\mathbf{d}_{B,GNL}, \tag{14}$$

and the spectral shape functions are determined by

$$\mathbf{N}_{B,GNL} = \mathbf{e}_{B,GNL}(x,\omega)\mathbf{H}^{-1}_{B,GNL}(\omega) = \left[\varphi_{B1,GNL}\ \varphi_{B2,GNL}\ \varphi_{B3,GNL}\ \varphi_{B4,GNL}\right], \tag{15}$$

which, for the sake of brevity, are not listed in detail here. From the relationships between the displacement and the bending moment $M(x) = -EIw''(x)$, as well as the transverse force $T(x) = -EIw'''(x) + Sw'(x)$, we obtain for the nodal forces $T_1 = -T(0)$, $M_1 = -M(0)$, $T_2 = T(l)$ and $M_2 = M(l)$

$$\begin{bmatrix} T_1 \\ M_1 \\ T_2 \\ M_2 \end{bmatrix} = \begin{bmatrix} -T(0) \\ -M(0) \\ T(l) \\ M(l) \end{bmatrix} = \begin{bmatrix} EIw'''(0) - Sw'(0) \\ EIw''(0) \\ -EIw'''(l) + Sw'(l) \\ -EIw''(l) \end{bmatrix}. \tag{16}$$

Substituting the displacement field from Eq. (14) with the shape functions from Eq. (15) into Eq. (16) finally yields

$$\begin{aligned} \begin{bmatrix} T_1 \\ M_1 \\ T_2 \\ M_2 \end{bmatrix} = \Bigg(& EI \begin{bmatrix} \varphi'''_{B1,GNL}(0) & \varphi'''_{B2,GNL}(0) & \varphi'''_{B3,GNL}(0) & \varphi'''_{B4,GNL}(0) \\ \varphi''_{B1,GNL}(0) & \varphi''_{B2,GNL}(0) & \varphi''_{B3,GNL}(0) & \varphi''_{B4,GNL}(0) \\ -\varphi'''_{B1,GNL}(l) & -\varphi'''_{B2,GNL}(l) & -\varphi'''_{B3,GNL}(l) & -\varphi'''_{B4,GNL}(l) \\ -\varphi''_{B1,GNL}(l) & -\varphi''_{B2,GNL}(l) & -\varphi''_{B3,GNL}(l) & -\varphi''_{B4,GNL}(l) \end{bmatrix} \\ & + S \begin{bmatrix} -\varphi'_{B1,GNL}(0) & -\varphi'_{B2,GNL}(0) & -\varphi'_{B3,GNL}(0) & -\varphi'_{B4,GNL}(0) \\ 0 & 0 & 0 & 0 \\ \varphi'_{B1,GNL}(l) & \varphi'_{B2,GNL}(l) & \varphi'_{B3,GNL}(l) & \varphi'_{B4,GNL}(l) \\ 0 & 0 & 0 & 0 \end{bmatrix} \Bigg) \begin{bmatrix} w_1 \\ \theta_1 \\ w_2 \\ \theta_2 \end{bmatrix}, \end{aligned} \tag{17}$$

where the expression in the brackets $(\bullet)$ is the spectral element matrix of the Euler-Bernoulli beam according to the geometrically nonlinear theory and can be written as

$$\mathbf{S}_{B,GNL} = \begin{bmatrix} s_{B11,GNL} & s_{B12,GNL} & s_{B13,GNL} & s_{B14,GNL} \\ s_{B21,GNL} & s_{B22,GNL} & s_{B23,GNL} & s_{B24,GNL} \\ s_{B31,GNL} & s_{B32,GNL} & s_{B33,GNL} & s_{B34,GNL} \\ s_{B41,GNL} & s_{B42,GNL} & s_{B43,GNL} & s_{B44,GNL} \end{bmatrix}. \tag{18}$$

The elements of the spectral element matrix $\mathbf{S}_{B,GNL}$, taking into account the symmetry property $s_{Bij,GNL} = s_{Bji,GNL}$ and the abbreviations $\overline{S} = S/EI$, $\bar{l}_1 = k_{\lambda_1} l$ and $\bar{l}_2 = k_{\lambda_2} l$, are given by

$$
\begin{aligned}
s_{B11,GNL} = &-\frac{EI}{\Delta_{11}} k_{\lambda1} k_{\lambda2} \left(k_{\lambda1}^2 + k_{\lambda2}^2\right) \Big(3k_{\lambda1}^2 k_{\lambda2} \sin\left(2\bar{l}_1\right) - k_{\lambda1}^3 \sinh\left(2\bar{l}_2\right) - k_{\lambda2}^3 \sin\left(2\bar{l}_1\right) \\
&+ 3k_{\lambda1} k_{\lambda2}^2 \sinh\left(2\bar{l}_2\right) + k_{\lambda1}^3 \cos\left(2\bar{l}_1\right) \sinh\left(2\bar{l}_2\right) + k_{\lambda2}^3 \cosh\left(2\bar{l}_2\right) \sin\left(2\bar{l}_1\right) \\
&- 8k_{\lambda1} k_{\lambda2}^2 \cos\left(\bar{l}_1\right) \sinh\left(\bar{l}_2\right) - 8k_{\lambda1}^2 k_{\lambda2} \cosh\left(\bar{l}_2\right) \sin\left(\bar{l}_1\right) + k_{\lambda1} k_{\lambda2}^2 \cos\left(2\bar{l}_1\right) \sinh\left(2\bar{l}_2\right) \\
&+ k_{\lambda1}^2 k_{\lambda2} \cosh\left(2\bar{l}_2\right) \sin\left(2\bar{l}_1\right) \Big), \\
\text{with } \Delta_{11} = &\, k_{\lambda1}^4 - k_{\lambda2}^4 \cos\left(2\bar{l}_1\right) - k_{\lambda1}^4 \cosh\left(2\bar{l}_2\right) - k_{\lambda2}^4 \cosh\left(2\bar{l}_2\right) - k_{\lambda1}^4 \cos\left(2\bar{l}_1\right) + k_{\lambda2}^4 + 18k_{\lambda1}^2 k_{\lambda2}^2 \\
&+ k_{\lambda1}^4 \cos\left(2\bar{l}_1\right) \cosh\left(2\bar{l}_2\right) + k_{\lambda2}^4 \cos\left(2\bar{l}_1\right) \cosh\left(2\bar{l}_2\right) + 6k_{\lambda1}^2 k_{\lambda2}^2 \cos\left(2\bar{l}_1\right) \\
&+ 6k_{\lambda1}^2 k_{\lambda2}^2 \cosh\left(2\bar{l}_2\right) - 32k_{\lambda1}^2 k_{\lambda2}^2 \cos\left(\bar{l}_1\right) \cosh\left(\bar{l}_2\right) + 2k_{\lambda1}^2 k_{\lambda2}^2 \cos\left(2\bar{l}_1\right) \cosh\left(2\bar{l}_2\right), \\
s_{B12,GNL} = &\, \frac{EI}{\Delta_{12}} \Big[k_{\lambda1}^6 - k_{\lambda2}^6 + \overline{S} k_{\lambda1}^4 + \overline{S} k_{\lambda2}^4 - k_{\lambda1}^6 \cos\left(2\bar{l}_1\right) + k_{\lambda2}^6 \cos\left(2\bar{l}_1\right) - k_{\lambda1}^6 \cosh\left(2\bar{l}_2\right) \\
&+ k_{\lambda2}^6 \cosh\left(2\bar{l}_2\right) - \overline{S} k_{\lambda1}^4 \cos\left(2\bar{l}_1\right) - \overline{S} k_{\lambda2}^4 \cos\left(2\bar{l}_1\right) - \overline{S} k_{\lambda1}^4 \cosh\left(2\bar{l}_2\right) - \overline{S} k_{\lambda2}^4 \cosh\left(2\bar{l}_2\right) \\
&- 9(k_{\lambda1}^2 k_{\lambda2}^4 - k_{\lambda1}^4 k_{\lambda2}^2 - 2\overline{S} k_{\lambda1}^2 k_{\lambda2}^2) - \cos\left(\bar{l}_1\right) \cosh\left(\bar{l}_2\right) \left(16k_{\lambda1}^4 k_{\lambda2}^2 - EI k_{\lambda1}^2 k_{\lambda2}^4 \right. \\
&\left. + 32\overline{S} k_{\lambda1}^2 k_{\lambda2}^2\right) + k_{\lambda1}^6 \cos\left(2\bar{l}_1\right) \cosh\left(2\bar{l}_2\right) - k_{\lambda2}^6 \cos\left(2\bar{l}_1 l\right) \cosh\left(2\bar{l}_2\right) \\
&+ \overline{S} k_{\lambda1}^4 \cos\left(2\bar{l}_1\right) \cosh\left(2\bar{l}_2\right) + \overline{S} k_{\lambda2}^4 \cos\left(2\bar{l}_1\right) \cosh\left(2\bar{l}_2\right) - 3k_{\lambda1}^2 k_{\lambda2}^4 \cos\left(2\bar{l}_1\right) \\
&+ 3k_{\lambda1}^4 k_{\lambda2}^2 \cos\left(2\bar{l}_1\right) - 3k_{\lambda1}^2 k_{\lambda2}^4 \cosh\left(2\bar{l}_2\right) + 3k_{\lambda1}^4 k_{\lambda2}^2 \cosh\left(2\bar{l}_2\right) + 6\overline{S} k_{\lambda1}^2 k_{\lambda2}^2 \cos\left(2\bar{l}_1\right) \\
&+ 6\overline{S} k_{\lambda1}^2 k_{\lambda2}^2 \cosh\left(2\bar{l}_2\right) - 4k_{\lambda1} k_{\lambda2}^5 \sin\left(\bar{l}_1\right) \sinh\left(\bar{l}_2\right) - 4k_{\lambda1}^5 k_{\lambda2} \sin\left(\bar{l}_1\right) \sinh\left(\bar{l}_2\right) \\
&+ k_{\lambda1} k_{\lambda2}^5 \sin\left(2\bar{l}_1\right) \sinh\left(2\bar{l}_2\right) + k_{\lambda1}^5 k_{\lambda2} \sin\left(2\bar{l}_1\right) \sinh\left(2\bar{l}_2\right) - k_{\lambda1}^2 k_{\lambda2}^4 \cos\left(2\bar{l}_1\right) \cosh\left(2\bar{l}_2\right) \\
&+ k_{\lambda1}^4 k_{\lambda2}^2 \cos\left(2\bar{l}_1\right) \cosh\left(2\bar{l}_2\right) + 2\overline{S} k_{\lambda1}^2 k_{\lambda2}^2 \cos\left(2\bar{l}_1\right) \cosh\left(2\bar{l}_2\right) \\
&- 8k_{\lambda1}^3 k_{\lambda2}^3 \sin\left(\bar{l}_1\right) \sinh\left(\bar{l}_2\right) + 2k_{\lambda1}^3 k_{\lambda2}^3 \sin\left(2\bar{l}_1\right) \sinh\left(2\bar{l}_2\right) \Big], \\
\text{with } \Delta_{12} = &\, 2k_{\lambda1}^4 - 2k_{\lambda2}^4 \cosh^2\left(\bar{l}_2\right) - 2k_{\lambda1}^4 \cos\left(2\bar{l}_1\right) - 2k_{\lambda2}^4 \cos\left(2\bar{l}_1\right) - 2k_{\lambda1}^4 \cosh^2\left(\bar{l}_2\right) + 2k_{\lambda2}^4 \\
&+ 12k_{\lambda1}^2 k_{\lambda2}^2 + 4k_{\lambda1}^2 k_{\lambda2}^2 \cos\left(2\bar{l}_1\right) + 2k_{\lambda1}^4 \cos\left(2\bar{l}_1\right) \cosh^2\left(\bar{l}_2\right) + 2k_{\lambda2}^4 \cos\left(2\bar{l}_1\right) \cosh^2\left(\bar{l}_2\right) \\
&+ 12k_{\lambda1}^2 k_{\lambda2}^2 \cosh^2\left(\bar{l}_2\right) - 32k_{\lambda1}^2 k_{\lambda2}^2 \cos\left(\bar{l}_1\right) \cosh\left(\bar{l}_2\right) + 4k_{\lambda1}^2 k_{\lambda2}^2 \cos\left(2\bar{l}_1\right) \cosh^2\left(\bar{l}_2\right), \\
s_{B13,GNL} = &\, \frac{1}{\Delta_{13}} \Big[4EI k_{\lambda1} k_{\lambda2} \mathrm{e}^{l(k_{\lambda2} + k_{\lambda1}\mathrm{i})} \left(k_{\lambda1} \sin\left(\bar{l}_1\right) + k_{\lambda2} \sinh\left(\bar{l}_2\right)\right) \left(k_{\lambda1}^2 + k_{\lambda2}^2\right) \Big], \\
\text{with } \Delta_{13} = &\, \mathrm{e}^{2\bar{l}_2} (k_{\lambda1} - k_{\lambda2}\mathrm{i})^2 \mathrm{i} - \left(k_{\lambda1}^2 - k_{\lambda2}^2\right) \left(\mathrm{e}^{2(\bar{l}_2 + \mathrm{i}\bar{l}_1)} + 1\right) \mathrm{i} + \mathrm{e}^{\bar{l}_1 2\mathrm{i}} (k_{\lambda1} - k_{\lambda2}\mathrm{i})^2 \mathrm{i} \\
&- 8k_{\lambda1} k_{\lambda2} \mathrm{e}^{l(k_{\lambda2} + k_{\lambda1}\mathrm{i})} + 2k_{\lambda1} k_{\lambda2} \left(\mathrm{e}^{2(\bar{l}_2 + \mathrm{i}\bar{l}_1)} + 1\right), \\
s_{B14,GNL} = &\, \frac{EI}{\Delta_{14}} \Big[k_{\lambda1} k_{\lambda2} \left(\cos\left(\bar{l}_1\right) - \cosh\left(\bar{l}_2\right)\right) \left(k_{\lambda1}^2 + k_{\lambda2}^2\right) \Big(2k_{\lambda1} k_{\lambda2} + k_{\lambda1}^2 \sin\left(\bar{l}_1\right) \sinh\left(\bar{l}_2\right) \\
&- k_{\lambda2}^2 \sin\left(\bar{l}_1\right) \sinh\left(\bar{l}_2\right) - 2k_{\lambda1} k_{\lambda2} \cos\left(\bar{l}_1\right) \cosh\left(\bar{l}_2\right) \Big) \Big], \\
\text{with } \Delta_{14} = &\, k_{\lambda1}^4 \cos^2\left(\bar{l}_1\right) \cosh^2\left(\bar{l}_2\right) - k_{\lambda1}^4 \cos^2\left(\bar{l}_1\right) - k_{\lambda1}^4 \cosh^2\left(\bar{l}_2\right) + k_{\lambda1}^4 + 2k_{\lambda1}^2 k_{\lambda2}^2 + k_{\lambda2}^4 \\
&+ 2k_{\lambda1}^2 k_{\lambda2}^2 \cos^2\left(\bar{l}_1\right) \cosh^2\left(\bar{l}_2\right) + 2k_{\lambda1}^2 k_{\lambda2}^2 \cos^2\left(\bar{l}_1\right) - 8k_{\lambda1}^2 k_{\lambda2}^2 \cos\left(\bar{l}_1\right) \cosh\left(\bar{l}_2\right) \\
&+ 2k_{\lambda1}^2 k_{\lambda2}^2 \cosh^2\left(\bar{l}_2\right) + k_{\lambda2}^4 \cos^2\left(\bar{l}_1\right) \cosh^2\left(\bar{l}_2\right) - k_{\lambda2}^4 \cos^2\left(\bar{l}_1\right) - k_{\lambda2}^4 \cosh^2\left(\bar{l}_2\right),
\end{aligned}
$$

$$
\begin{aligned}
s_{B22,GNL} = \frac{EI}{\Delta_{22}} \left(k_{\lambda1}^2 + k_{\lambda2}^2\right) \Big(& k_{\lambda1}^3 \sin\left(2\bar{l}_1\right) - k_{\lambda2}^3 \sinh\left(2\bar{l}_2\right) - 3k_{\lambda1}k_{\lambda2}^2 \sin\left(2\bar{l}_1\right) \\
& + 3k_{\lambda1}^2 k_{\lambda2} \sinh\left(2\bar{l}_2\right) - k_{\lambda1}^3 \cosh\left(2\bar{l}_2\right) \sin\left(2\bar{l}_1\right) + k_{\lambda2}^3 \cos\left(2\bar{l}_1\right) \sinh\left(2\bar{l}_2\right) \\
& + 8k_{\lambda1}k_{\lambda2}^2 \cosh\left(\bar{l}_2\right) \sin\left(\bar{l}_1\right) - 8k_{\lambda1}^2 k_{\lambda2} \cos\left(\bar{l}_1\right) \sinh\left(\bar{l}_2\right) - k_{\lambda1}k_{\lambda2}^2 \cosh\left(2\bar{l}_2\right) \sin\left(2\bar{l}_1\right) \\
& + k_{\lambda1}^2 k_{\lambda2} \cos\left(2\bar{l}_1\right) \sinh\left(2\bar{l}_2\right) \Big), \\
\text{with } \Delta_{22} = {} & k_{\lambda1}^4 - k_{\lambda2}^4 \cos\left(2\bar{l}_1\right) - k_{\lambda1}^4 \cosh\left(2\bar{l}_2\right) - k_{\lambda2}^4 \cosh\left(2\bar{l}_2\right) - k_{\lambda1}^4 \cos\left(2\bar{l}_1\right) + 18k_{\lambda1}^2 k_{\lambda2}^2 \\
& + k_{\lambda2}^4 + k_{\lambda1}^4 \cos\left(2\bar{l}_1\right) \cosh\left(2\bar{l}_2\right) + k_{\lambda2}^4 \cos\left(2\bar{l}_1\right) \cosh\left(2\bar{l}_2\right) - 32k_{\lambda1}^2 k_{\lambda2}^2 \cos\left(\bar{l}_1\right) \cosh\left(\bar{l}_2\right) \\
& + 6k_{\lambda1}^2 k_{\lambda2}^2 \cos\left(2\bar{l}_1\right) + 6k_{\lambda1}^2 k_{\lambda2}^2 \cosh\left(2\bar{l}_2\right) + 2k_{\lambda1}^2 k_{\lambda2}^2 \cos\left(2\bar{l}_1\right) \cosh\left(2\bar{l}_2\right).
\end{aligned}
$$

It should be noted that for a compressive force, the wavenumbers have to be chosen according to Eq. (8) and the axial force S has to be used with a negative sign. For a tensile force, the wave numbers in Eq. (9) have to be used and the positive sign applies to the axial force S. It should also be noted that the critical buckling load of a system can also be determined by the derived spectral element matrix $\mathbf{S}_{B,GNL}$. To do this, the angular frequency has to be set to $\omega = 0$ and an eigenvalue problem for the axial force S must be solved.
Finally, the spectral element matrices of the rod element, which can be found in the works of Doyle [7] or Lee [8], and the geometrically nonlinear beam element can be combined into a 6×6 extended spectral Euler-Bernoulli beam element matrix $\mathbf{S}_{EB,GNL}$ with the corresponding nodal degrees of freedom $[u_1\ w_1\ \theta_1\ u_2\ w_2\ \theta_2]^T$, where u_i are the nodal axial displacements.

3 CALCULATION OF THE COMPLEX BAND STRUCTURES

The band structures are calculated using a unit-cell with periodic Bloch-Floquet boundary conditions, where the investigations in this work are based on the unit-cell shown in Fig. 5a with the square cross-section shown in Fig. 5b. Due to the exact element matrices the discretization of the unit-cell into several elements is only required in the case of geometric discontinuities, such as at the kinks of the zig-zag lattice, and in the case of cross-section and material changes. For the following calculations the geometric parameters are set to $l = 100\,\mathrm{mm}$, $W = 10\,\mathrm{mm}$, $a = 2\,\mathrm{mm}$, and the material properties of aluminum with $E = 70\,\mathrm{GPa}$, $\rho = 2700\,\mathrm{kg/m^3}$ are used.

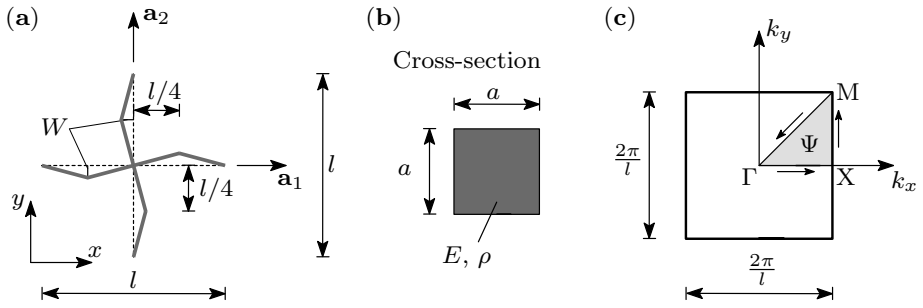

Figure 5: (**a**) Unit-cell of the phononic zig-zag lattice with the (**b**) cross-section of the zig-zag members. (**c**) First irreducible Brillouin zone of the unit-cell.

When calculating the complex band structures, a quadratic or quartic eigenvalue problem must be solved depending on the edge of the first irreducible Brillouin zone (IBZ) considered, which is shown in Fig. 5c. The exact procedure for calculating the complex band structures is described in detail in the work by Veres [9], for example, and is therefore not explained in detail here. An efficiency comparison between the SEM and the FEM for the calculation of the complex band structures can be made by evaluating the numerical errors of the FEM calculations for different numbers of degrees of freedom and the associated corresponding calculation times. The relative error ε_2 of the l_2 norm can be calculated for the band structure for each discrete frequency via

$$\varepsilon_2 = \sqrt{\sum_{n=1}^{N} \left(k_n - k_n^{ref}\right)^2} \Bigg/ \sqrt{\sum_{n=1}^{N} \left(k_n^{ref}\right)^2} \cdot 100, \tag{19}$$

where in this case k_n are the wave numbers of the FEM solutions and k_n^{ref} are the wave numbers of the SEM reference solution. The Fig. 6a shows the averaged errors $\bar{\varepsilon}_2$ of the FEM calculations, which are obtained by avererging the errors ε_2 of 1200 discrete frequencies. It is evident, that the errors are decreasing and the FEM solution is approaching the SEM reference solution with increasing number of degrees of freedom. However, the corresponding calculation time of the

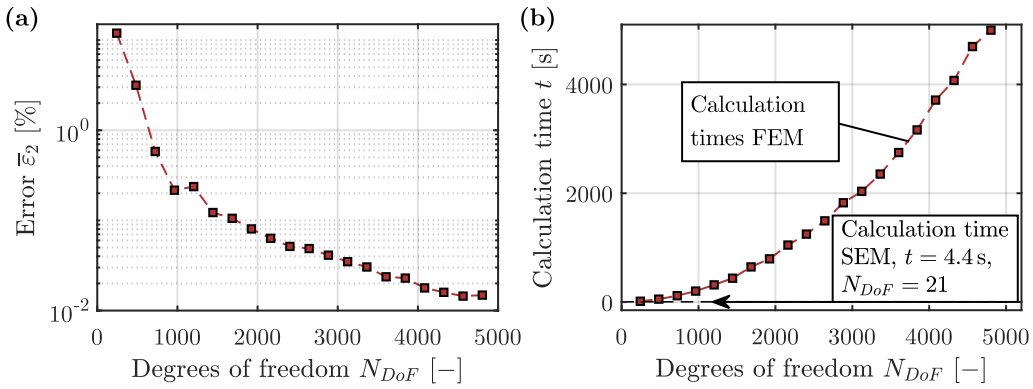

Figure 6: (**a**) Average errors $\bar{\varepsilon}_2$ of the FEM calculations for different numbers of degrees of freedom. (**b**) Corresponding calculation times for 1200 discrete frequency steps of the FEM for different numbers of degrees of freedom and the calculation time of the SEM for 21 degrees of freedom.

FEM, as shown in the Fig. 6b, is increasing exponentially with increasing number of degrees of freedom. In addition, the calculation time of the SEM solution for 21 degrees of freedom is also shown in Fig. 6b, which is extremely low with $t = 4.4\,\mathrm{s}$. Considering the very low calculation time of the SEM which at the same time yields exact solutions, the clear advantage of the SEM compared to the FEM becomes evident. The calculated complex band structures are shown in the Fig. 7, where the real part of the wave vector is shown on the left, the imaginary part is shown in the middle and the corresponding transmission spectrum of a finite-sized periodic structure consisting of 8 unit-cells in the y-direction and 16 unit-cells in the x-direction is shown on the right. From the band structures it can be seen that the zig-zag lattice structure has 3 band-gaps in the considered frequency range. The smallest imaginary part of the wave vector is always zero outside of the band-gaps and always larger than zero inside the band-gaps. The

smallest imaginary part of the wave vector is an important indicator for the damping behavior of a finite-sized periodic structure since it characterizes the least rapidly decaying wave. The transmission spectrum on the right shows that the transmission falls off rapidly within the frequency range of a band-gap and the vibration is very strongly damped. For more details on the calculation of the transmission spectra we refer to [3].

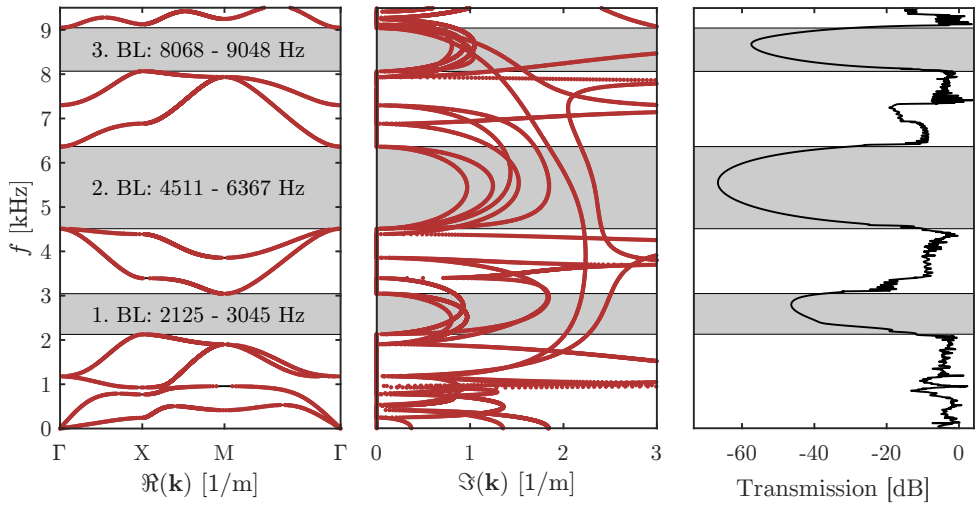

Figure 7: Complex band structures of the unit-cell shown in Fig. 5 and transmission spectrum of a finite-sized periodic structure consisting of 8 unit-cells in the y-direction and 16 unit-cells in the x-direction.

4 INFLUENCES OF THE GEOMETRICAL NONLINEARITY

The following investigations are based on the unit-cell shown in Fig. 5 with the geometric parameters $l = 100\,\text{mm}$, $W = 10\,\text{mm}$, $a = 2\,\text{mm}$, and the material parameters $E = 70\,\text{GPa}$, $\rho = 2700\,\text{kg/m}^3$. Figure 8 shows the influence of the axial frequencies of the first band-gap. The

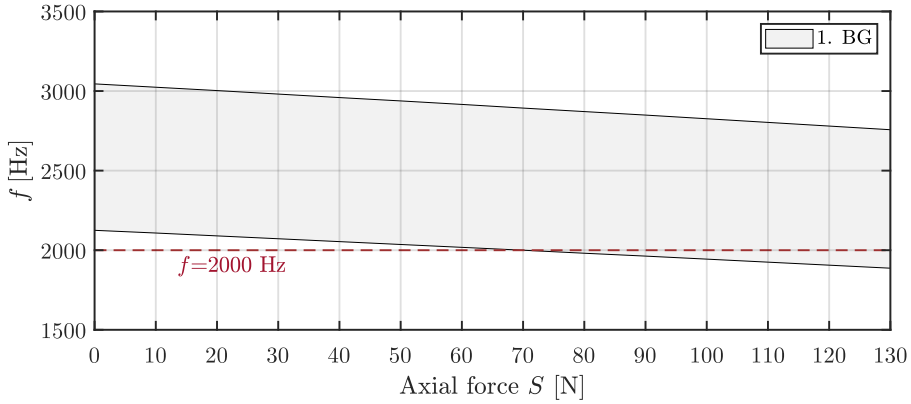

Figure 8: Influence of the axial compressive force S on the band-gap edge frequencies of the first band-gap.

calculations are based on a biaxial load condition, where all beams of the lattice have the same axial force S. In addition, only axial forces below the first local buckling load are considered, which means that the influences from the geometric nonlinearity remain reversible. Figure 8 shows that applying an axial compressive force of $S = 130\,\mathrm{N}$ can reduce the edge frequencies by about 200 Hz. For the lower edge frequency of the first band-gap, this corresponds to a reduction of around 10%. To illustrate the influence of the geometric nonlinearity, the frequency of $f = 2000\,\mathrm{Hz}$ is marked in Fig. 8, which is outside the band-gap for $S = 0\,\mathrm{N}$ (without geometric nonlinearity) and inside the band-gap for $S = 130\,\mathrm{N}$ (with geometric nonlinearity). The corresponding displacement field in the frequency domain for the case $S = 0\,\mathrm{N}$ (without

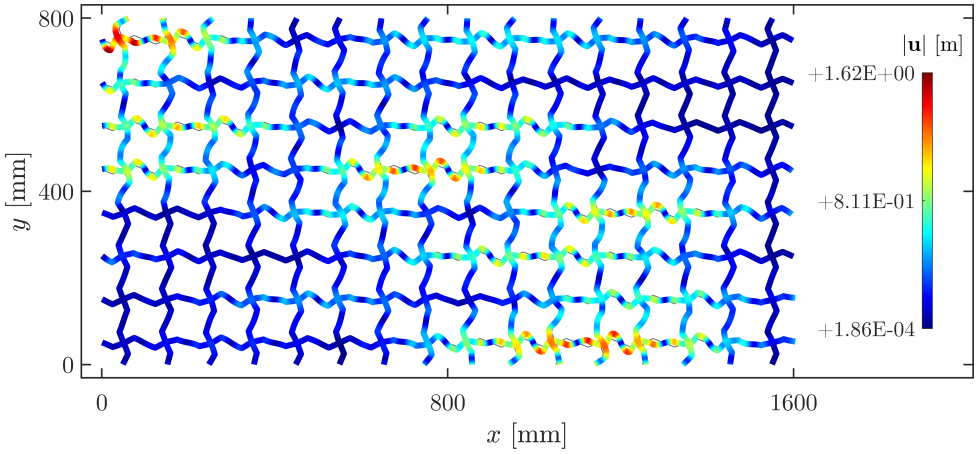

Figure 9: Displacement field in the frequency domain for $f = 2000\,\mathrm{Hz}$ and $S = 0\,\mathrm{N}$ (without geometric nonlinearity). TThe structure is excited on the left boundary by the prescribed displacement $\mathbf{u}_0 = [0.1\ 0.1]^T$ m.

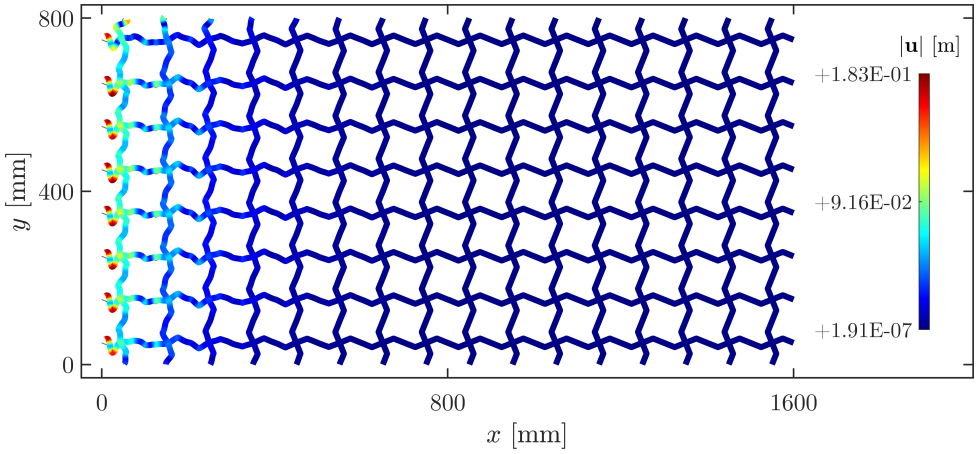

Figure 10: Displacement field in the frequency domain for $f = 2000\,\mathrm{Hz}$ and $S = 130\,\mathrm{N}$ (with geometric nonlinearity). The structure is excited on the left boundary by the prescribed displacement $\mathbf{u}_0 = [0.1\ 0.1]^T$ m.

geometric nonlinearity) is shown in Fig. 9, where the finite-sized lattice structure is excited on the left boundary with a prescribed displacement $\mathbf{u}_0 = [0.1\ 0.1]^T$ m. It is obvious that the vibrations or elastic waves can propagate in the lattice structure without being damped. On the other hand, the displacement field in the frequency domain for the case $S = 130\,\mathrm{N}$ (with geometric nonlinearity), which is shown in Fig. 10, shows that the vibrations cannot propagate in the lattice structure and are strongly attenuated.
Finally, the influence of the axial force S on the damping behavior of the phononic zig-zag lattice structure is also investigated. Fig. 11 shows the influence of the axial force on the smallest imaginary part of the wave vector at the band-gap center frequencies and the associated elastic wave transmission. It turns out that the axial force S, in contrast to other parameters such as the deflection W, has no significant influence on the smallest imaginary part of the wave vector and the elastic wave transmission of the phononic zig-zag lattice structure. Consequently, the damping behavior of the phononic lattice structure is neither improved nor deteriorated significantly by considering axial forces. However, the presented examples show, that the band-gap frequency ranges of the phononic lattice structures can be adaptively influenced by utilizing the effects of the geometric nonlinearity.

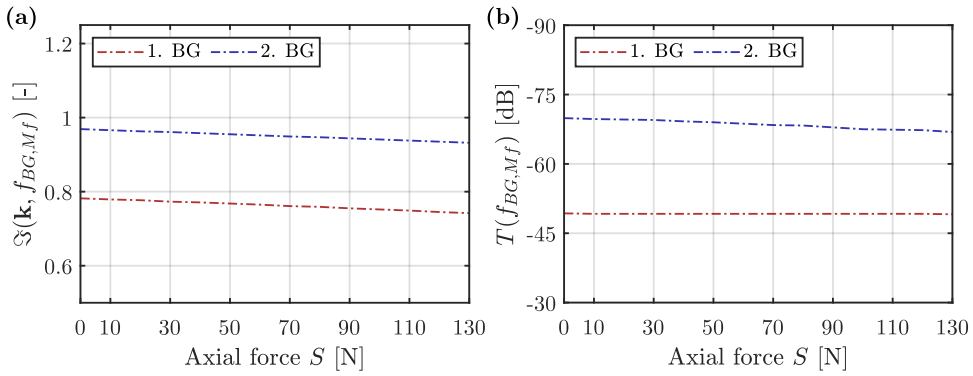

Figure 11: Influence of the axial compressive force S on the (**a**) smallest imaginary part of the wave vector at the band-gap center frequencies and (**a**) on the corresponding elastic wave transmission.

5 CONCLUSIONS

The SEM is a very efficient numerical method to compute the complex band structures, which give valuable information about the evanescent bahavior of the Bloch waves, and the transmission spectra of periodic lattice structures. It can provide highly accurate results with a reasonable computing time. The band-gaps of phononic zig-zag lattice structures can be tuned by the geometric parameters (deflection W, lattice constant l, cross-sectional parameters, etc.) and adaptive vibration or elastic wave filters can be designed by utilizing the effects of the geometric nonlinearity.

REFERENCES

[1] Liu, J. and Guo, H. and Wang, T.: A review of acoustic metamaterials and phononic crystals. *Crystals* (2020), **10**(4):305.

[2] Matlack, K. H. and Bauhofer, A. and Krödel, S. and Palermo, A. and Daraio, C.: Composite 3D-printed metastructures for lowfrequency and broadband vibration absorption. *Proceedings of the National Academy of Sciences of the United States of America* (2016), **113**:8386–8390.

[3] Mellmann, M. and Perras, E. and Zhang, C.: Computation of the elastic wave band structures and transmission in pre-deformed periodic frame structures by SEM. *Proceedings of Forum Acusticum 2020* (2020), DOI: 10.48465/fa.2020.0358, 1117–1123.

[4] Mellmann, M. and Zhang, C.: Tuning of vibration and wave propagation characteristics in pre-deformed periodic lattice frame structures. *Proceedings in Applied Mathematics and Mechanics 19* (2019), DOI: 10.1002/pamm.201900291.

[5] Banerjee, J. R. and Fisher, S. A.: Coupled bending-torsional dynamic stiffness matrix for axially loaded beam elements. *International Journal for Numerical Methods in Engineering* (1992), **33**(4):739–751.

[6] Capron, M. D. and Williams, F. W.: Exact dynamic stiffnesses for an axially loaded uniform Timoshenko member embedded in an elastic medium. *Journal of Sound and Vibration* (1988), **124**(3):453–466.

[7] Doyle, J. F.: *Wave Propagation in Structures – Spectral Analysis Using Fast Discrete Fourier Transforms*. Springer Science + Business Media, New York, 2. Ed., (1997).

[8] Lee, U.: *Spectral Element Method in Structural Dynamics*. John Wiley & Sons (Asia) Pte Ltd, Singapur, 1. Ed., (2009).

[9] Veres, I. A. and Berer, T. and Matsuda, O.: Complex band structures of two dimensional phononic crystals: Analysis by the finite element method. *Journal of Applied Physics* (2013), **114**(8):083519.